Reprinted from Nature, Vol. 297, No. 5867, pp. 563-568, 17 June 1982

Structure of the expanded state of tomato bushy stunt virus

I. K. Robinson & S. C. Harrison

Gibbs Laboratory, Harvard University, Cambridge, Massachusetts 02138, USA

The full three-dimensional structure determination of tomato bushy stunt virus has shown how its protein subunit can accommodate to different packing environments in the viral coat and how the size of the particle is nonetheless determined without ambiguity. Reversible, cooperative expansion of the virus at pH values above neutrality and in the absence of divalent cation requires further bonding alternatives for the subunit. We report here the structure of the expanded tomato bushy stunt virus particle, determined at 8 Å resolution by X-ray crystallography. Subunit conformational changes are localized, and folded domains are essentially invariant. The bonding properties of the subunit can account for controlled polymorphism of the assembly.

THE tomato bushy stunt virus (TBSV) particle comprises a single strand of RNA (molecular weight (M_r) 1.5×10^6) and 180 copies of a 40,000 M_r coat protein[1]. The subunits of the coat are arranged in a $T = 3$ icosahedral lattice[2] as shown in Fig. 1*a*. High-resolution crystal structure analysis[3] has revealed the positions of all amino-acid residues in the C-terminal 75% of the protein chains; these form a shell having inner and outer radii of 110 and 170 Å. The N-terminal parts of the protein subunits and the whole of the RNA are invisible in the icosahedrally averaged, high-resolution electron density maps; they are thus believed to be spatially disordered. These components together fill the cavity in the interior of the virus[4,5].

The ordered part of the protein folds into two structural domains linked by a short 'hinge'. The 170-amino acid 'S'-domains pack tightly into the shell between radii of 110 and 140 Å. The three symmetrically distinct positions of this domain, shown in Fig. 1*b*, are denoted A, B and C. They have identical folding of their polypeptide backbone, but adjust to three 'quasi-equivalent' environments by differences in conformation of certain side chains on their surfaces and, more dramatically, by the ordered folding of 35 residues at the N-terminal end of the 60 C-position S-domains. These 35 residues form the so-called 'extended arm' and 'β-annulus'[3]. The A- and B-position S-domains make an extensive contact with each other, which is broken in C positions by interposition of the arm. Distal residues of the arm interdigitate with corresponding residues of two other C subunits to form the β-annuli. A coherent internal scaffold is thereby created, which precisely determines the curvature and size of the virus particle.

The second domain, called 'P', forms strong dimers that lie on the 2-fold and quasi-2-fold axes of the constellation of S-domains. These dimers project to the outer radius of 170 Å and are clearly visible in electron micrographs of the virus[6].

Expansion

TBSV and many other related viruses undergo a structural phase transition in solution that is controlled primarily by *p*H and divalent cation concentration. The phenomenon was first observed in bromegrass mosaic virus (BMV) by Incardona and Kaesberg[7] using various physicochemical techniques. These all gave results consistent with a model in which the particle mass was conserved and the hydrodynamic radius increased by ~10%. For this reason we will refer to it as 'expansion' of the virus.

BMV exhibits an anomalous titration of two protons per subunit associated with the phase transition at *p*H 6.7. This has been interpreted[8,9] as due to formation of hydrogen bonds between apposed carboxylic acid groups. Divalent cations, known to inhibit the expansion of BMV, would displace the hydrogen bonds in favour of ionic links stable at all *p*H values. Native preparations of TBSV have two bound, EDTA-chelatable ions per subunit (probably both calcium) which must be removed before expansion can be observed[10]. Once free of these ions, the virus expands reversibly when the *p*H is raised above 7.0; the transition seems to be characterized by some hysteresis, which is most easily followed by changes in the solution X-ray scattering. The location and structure of the cation binding sites[11] are consistent with the mechanism just described: five aspartate side chains, contributed by each pair of adjacent S-domains in the trimer of Fig. 1*b*, are involved in the binding of the two ions. When charged at high *p*H, these aspartates repel each other and destabilize the inter-domain contact. This interface is therefore likely to be the one broken to permit expansion.

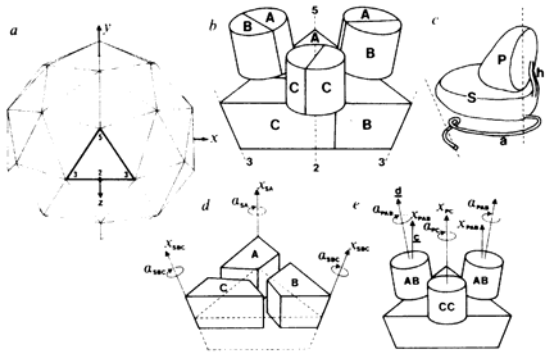

Fig. 1 Architecture of the TBSV particle as determined by high-resolution X-ray structure analysis, and model of its expansion. *a*, Stellated pentagonal dodecahedron showing the definition of the icosahedral asymmetric unit (highlighted) as the spherical sector lying between a 5-fold and two adjacent 3-fold axes. The viral shell consists of 60 of these identical units. *b*, Schematic diagram showing the packing of three quasi-equivalent TBSV protein subunits in the icosahedral asymmetric unit, denoted A, B and C. *c*, Approximate shape of the C-position subunit, showing the two domains, denoted 'S' (surface) and 'P' (projecting), connected by a polypeptide hinge, h. The N-terminal arm, a, is ordered only in the C-position subunit and disordered in A and B. *d*, Parameterization of the model of the expansion of the S-domains. A translation, x, parallel to the symmetry axis and a rotation, α, about that axis is the most general description. The B- and C-position domains are assumed to retain their contacts about the 3-fold axis and so are described by the same parameter pair. *e*, Parameterization of the P-domain expansion. The AB P-domain dimer is unconstrained by the particle symmetry, and so has the full six parameters of a rigid body transformation. Spherical polar coordinates are used for compatibility with the other parameter definitions.

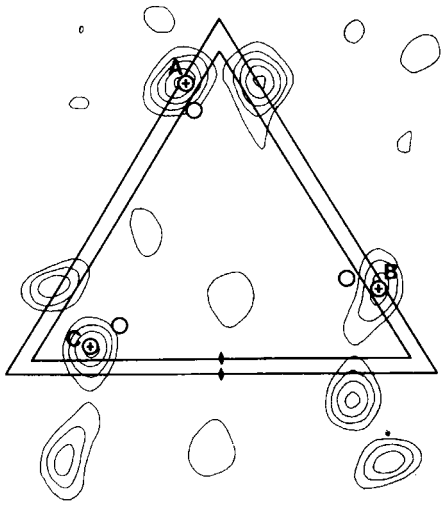

Fig. 2 A section of the 12 Å difference Fourier for the $PtCl_4$ derivative, located 132 Å from the particle centre. Phases for this map were derived from the best three-parameter model and refined by symmetry averaging. The larger triangle denotes the boundary of the icosahedral asymmetric unit and the symbol ⊕ denotes the refined atomic positions. The quasi-symmetry of these site positions is clearly apparent. Superimposed on the same scale are the refined platinum positions for the compact virus (○), which lie at a radius of ~116 Å, and the size of the icosahedral asymmetric unit at that radius (smaller triangle). The vector joining the platinum position in the compact virus to that of the expanded virus is an accurate measure of the displacement of the subunit to which the atom is bound.

Examination of the relative extent of various contacts between S-domains in the high-resolution structure[3,11] led to a model for expansion, shown in Fig. 1*d*. This model assumed that the virus retained its icosahedral symmetry and that the internal tertiary structure of each domain was conserved. Rapid reversibility of expansion further suggested that the interlocked internal scaffold was conserved and hence that the pentamer and hexmer clusterings of S-domains in the virus were unaltered. As argued above, it was reasonable to suppose that the trimer contacts, which contain the divalent cation sites, were disrupted. With this model, S-domain displacements can be described by just four parameters, two rotations about and two translations along the symmetry axes. The motions of the P-domains described in Fig. 1*e* are rather more general: only the PP dimer contact is conserved, so eight parameters make a complete description. We have used this model-building approach in the crystal structure determination.

Structure determination

Crystals of the expanded virus were prepared by vapour diffusion[12] from 2.9% polyethylene glycol, 0.01 M EDTA, 0.058 M $(NH_4)_2HPO_4$, 20% ethylene glycol, *p*H 7.5 at 18 °C. X-ray diffraction showed crystalline order to ~7 Å resolution. The space group is C2, with cell constants $a = 546.3$ Å, $b = 433.1$ Å, $c = 383.4$ Å and $\beta = 134.0°$. The crystallographic asymmetric unit contains one half of a virus particle, so there is 30-fold non-crystallographic symmetry, which can be exploited for refinement of phases[13]. The particle position within the unit cell is defined in this space group with the exception of the particle orientation angle about the 2-fold axis, referred to as θ, which must be determined experimentally; an additional parameter must therefore be added to the model description of the expanded virus in the crystals.

Data were collected by oscillation photography[14] for native crystals as well as $PtCl_4^{2-}$ and ethyl mercury thiosalicylate (EMTS) heavy-atom derivatives. These heavy-atom reagents were similar to those used in the structure determination of the compact virus[15], in the hope that the same sites would be labelled and a direct comparison of coordinates could be made. The data quality deteriorated sharply with resolution, and only reflections in the range 8–35 Å were considered usable. Table 1*a* summarizes native and derivative data collection. Comparison of Wilson plots for data from the compact and expanded forms of the virus indicated that the absence of high-resolution data for the latter was well modelled by gaussian disorder, with a Debye 'temperature factor' of 340 $Å^2$.

Starting values of the model parameters were obtained by analysing the packing of the expanded virus particles into the crystal unit cell. These were used to compute a predicted diffraction pattern, which was compared with the observed pattern by calculating an *R*-factor for agreement of scaled

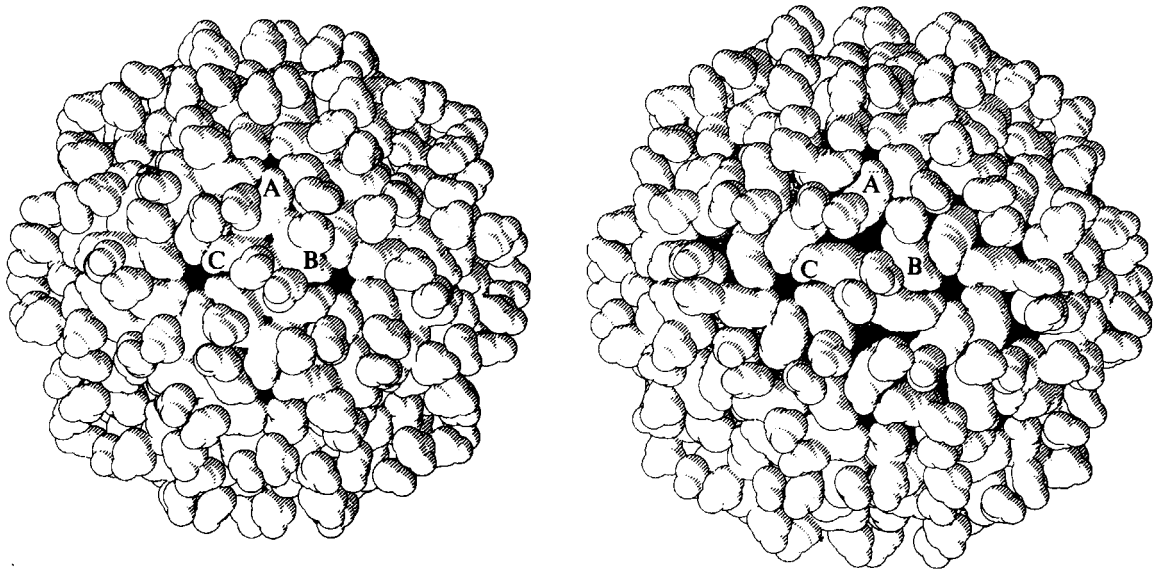

Fig. 3 Pictorial view of the expansion of TBSV. The compact particle is on the left. Note the appearance of the inter-subunit opening and the rotation of the projecting domains in the expanded virus on the right. (This figure was prepared by A. J. Olson using a modified form of the PLUTO program of S. Motherwell.)

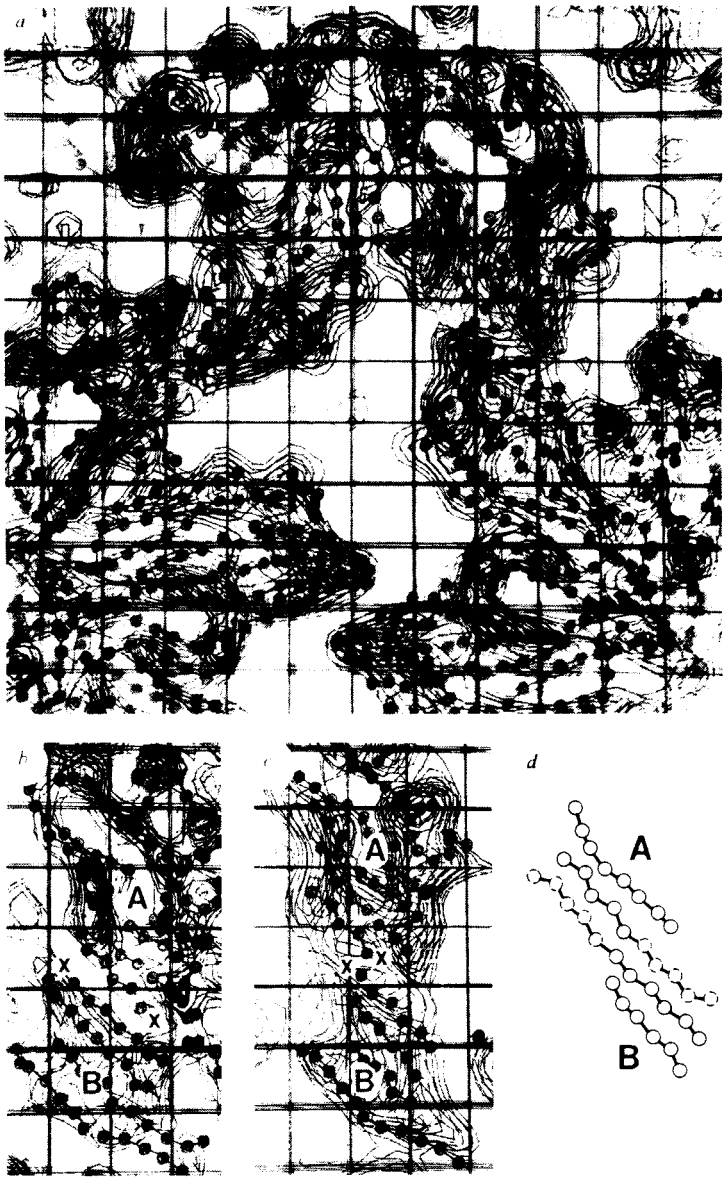

Fig. 4 Electron density maps at 8 Å resolution and their interpretation. Dots are superimposed for each amino acid in the best-fitting model of the expanded virus. The grid is 10 Å square. *a*, Overall view of the icosahedral asymmetric unit of expanded TBSV in the S-domain region. The opening is clearly visible between the domains. An impression of the quality of the map can be obtained from the fit of model to density and from the noise level in the solvent regions. *b*, The contact between the A and B position S-domains of the compact structure. The residue marked 'X' in each subunit is the first residue to be included at the N-terminus of the model. This part of the structure contains a four-strand antiparallel β-sheet extending across the base of the domain. *c*, The corresponding region of the expanded structure in which the two domains are shifted past each other by 14 Å. There is clear density immediately preceding residue X which can be interpreted as an ordering of the arm. *d*, Interpretation of the new electron density as an additional strand of β-sheet that forms a clamp between the subunits.

intensities. The model parameters were adjusted until the *R*-factor was minimized. A value of $R=0.52$ was obtained for 12 Å, significantly lower than the value of 0.59 obtained by comparing sets of uncorrelated intensities. A more detailed account of this critical step and of the rest of the structure determination will be published elsewhere.

Phases calculated from the best model were applied to the observed structure facors to 12 Å resolution and subjected to refinement by non-crystallographic symmetry averaging[13]. The *R*-factor for comparison of symmetry-averaged and observed intensities was reduced to 0.38 in six cycles (12 Å data) and the phases on average moved by 55°.

To confirm the validity of the phasing and to extend its resolution, heavy-atom difference maps were calculated for both derivatives using the refined 12 Å phases. An example is shown in Fig. 2. Sites corresponding to the three platinum positions[15] were unambiguously identified. Their parameters were refined by conventional methods[16]. The *a priori* assumptions of rigid-body domain motion and conservation of hexamer and pentamer subunit contacts were supported by the finding that the positions of the S-domain heavy-atom sites were self-consistent to within 2 Å (Table 1*b*). The refined positions allowed a considerably more precise set of model parameters to be derived directly.

The three steps of model-building, *R*-factor minimization and non-crystallographic symmetry phase refinement were then repeated to extend the phasing to the full 8 Å data set. The refined heavy-atom occupancies at 8 Å were unchanged from their values at 12 Å (Table 1*b*), indicating the absence of significant deviations from icosahedral symmetry. Fourier analysis of the best model gave an *R*-factor of 0.46 with all the observed data. Phase refinement brought this value down to 0.43; the lack of dramatic improvement here indicates that the model description is a good one and reflects the poorer quality of the higher-resolution data. Electron density maps were prepared with dots superimposed for every amino acid residue of the model structure. Corresponding 8 Å maps of the compact structure with an imposed 340 Å^2 'temperature factor' were also prepared for comparison.

Interpretation of electron density

The successful refinement and correct determination of heavy-atom positions confirm our assumption that tertiary structure

in each domain is conserved, with conformational changes restricted to localized flexible regions. The displacements and rotations generated by these local flexions are described by the refined model parameters in Table 2. A striking aspect of the expanded state is the appearance of a branched opening 80 Å long and large enough for a 20 Å sphere to pass through each of the 60 faces; this is seen in Fig. 3, and an overall view of the icosahedral asymmetric unit is shown in Fig. 4*a*. The P-domains are rotated by relatively large angles, 30° in the AB case and 103° for the CC dimer. This latter value is so great that the actual direction of the rotation is ambiguous; the clockwise direction is chosen on the basis of a more reasonable conformation of the hinge. To accommodate these rotations and to bridge the gap between the domains, it is necessary to postulate a new 'expansion hinge', several residues long, to the N-terminal side of the hinge associated with the quasi-symmetry[3]. We have thus seen four distinct states of the linkage region between S- and P-domains: in A/B and in C positions in each of the compact and expanded particles.

The refined expansion parameters and the known high-resolution structures of the individual domains define an accurate model of the expanded virus. Use of this model greatly facilitated further interpretation of the refined electron density. Even though the resolution was not sufficient to distinguish individual strands of protein, the fit of model to density was good enough for small changes from the model to be detected reliably.

The extended arm, which is ordered in C-position S-domains but not in A or B, is conserved in the expanded virus, as is the β-annulus. The latter feature is much stronger in the expanded form; it appears ordered for several residues further into the interior of the virus. The function of the C-position arm and the β-annulus is to determine the size of the virus during assembly[3,11]. Conservation of these features in the expanded state is consistent with their fundamental role in establishing structural coherence.

The contact between the four-stranded β-sheets at the base of the A- and B-position S-domains is sheared apart by the expansion, as shown in Fig. 4*b* and *c*. A very distinct bulge of new density lies beside the first strand in both the A and B positions of the expanded state. This seems to be additional ordered protein at the N-terminus of the domain, and we suggest the interpretation of Fig. 4*d*. About six residues immediately N-terminal to the A and B position, S-domains of the compact structure become ordered in the expanded state, extending the first strand of each β-sheet and forming hydrogen bonds with residues of the opposite subunit. This interaction would create a single large sheet extending across the inner surface of both S-domains (Fig. 5). The density is interpreted in this way as the new B-position arm extending beyond the base of the A-position S-domain for a further 20 Å along the inside edge of the inter-subunit opening, terminating at a radius of 156 Å, close to the exterior of the virus. Thus, one of the arms seems to pass all the way through the opening to the outside, possibly explaining the observation that mild proteolysis of expanded virus causes a cleavage of many of the chains at positions 70 to 100 residues from the N-terminus[17].

A feature of the S-domain also seems to have shifted during expansion. The trimer contact region in the centre of the triangular icosahedral asymmetric unit of the virus (see Fig. 1*b*) consists of three loops of extended chain in symmetrical contact. In the maps of expanded virus, the rigid model of the domain has no electron density in this region, while a new loop of density of equal contour length protrudes into the opening. We suggest that a local refolding of the chain occurs in this region, with a displacement of ~10 Å at the tip of the loop. A similar change in secondary structure of an exterior loop has been observed in trypsinogen[18].

Apart from this limited number of modifications, which are easily rationalized, the model of the expanded virus is completely consistent with the electron density. As all the density is accounted for, we are confident of the interpretation.

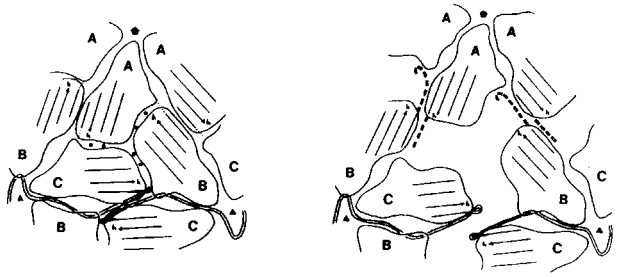

Fig. 5 Schematic diagrams showing the inner surface of S-domains in compact and expanded TBSV and indicating the interpreted disposition of the A and B position arms in the expanded structure. The Ca^{2+} sites are shown by pairs of dots[10]. The β-sheets at the base of the S-domains are denoted by four parallel lines, the C arms by double lines and the interpretation of A and B arms in expanded TBSV by broken lines. In this interpretation, the A arm extends to make a six-residue contact with the B subunit, and the B arm extends for about 15 residues, making the same 6-residue contact with the A subunit and continuing up the inside of the opening to the outside of the virus. The C arm has exactly the same conformation in both structures, except that in expanded virus it is ordered ~10 Å further into the viral interior. The strands terminating in arrows and indicated by 'h' lead to the inter-domain hinge. The change in spacing of these arrowheads across dyads when the particle expands illustrates the requirement for an 'expansion hinge' as described in the text.

Table 1 Data collection statistics for expanded TBSV (*a*) and refined heavy-atom coordinates (*b*)

a

Resolution limit (Å)	16	12	8	
No. of possible reflections	6,888	17,323	60,193	
No. observed	3,880	10,356	36,113	Native
R_{sym}	0.10	0.12	0.20	Native
No. observed	508	1,357	4,733	$PtCl_4$
R_{sym}	0.10	0.12	0.16	$PtCl_4$
No. observed	1,351	3,607	12,579	EMTS
R_{sym}	—	0.11	0.20	EMTS

b

	x	*y*	*z*	Occupancy (12 Å)	Occupancy (8 Å)
Platinum					
A	−8	67	134	8.1	8.0
B	37	19	133	6.4	7.2
C	−30	7	133	6.7	7.0
Mercury					
A1	−17	44	146	4.1	4.2
B1	19	40	145	4.5	2.9
C1	−5	9	145	3.2	2.7
A2	−29	48	178	2.2	4.5
B2	29	46	179	3.8	4.6
C2	10	5	179	2.1	2.2
E	−43	1	151	3.2	3.1

a, A total of 56 1° oscillation films were used in the final native data set. The reproducibility of the data is indicated for the redundant measurements by R_{sym}.

$$R_{sym} = \frac{\sum_h \sum_{j=1}^{n_h} |I_{hj} - \bar{I}_h|}{\sum_h n_h \bar{I}_h}$$

where the I_{hj}, $j = 1, \ldots n_h$ are the repeated measurements of I_h, and $\bar{I}_h$ is their mean. *b*, Refined heavy-atom coordinates (Å in coordinate frame of Fig. 1*a*) and relative occupancies (arbitrary units). Individual heavy-atom temperature factors were set to 25 Å^2 and not refined. Occupancies are shown for refinements at 12 Å and 8 Å resolution. All sites except E have chemically equivalent positions in the derivatives of compact TBSV, and their nomenclature corresponds to that of Table 2 in ref. 15. Site E is unique to the expanded structure and lies near a known cysteine.

Stability and disorder in the expanded structure

The detailed interpretation of electron density described above shows that the expanded state is characterized by a relatively rigid network of S-domains. This network may be stabilized in part by a new contact between the bases of the A and B S-domains, involving an ordered conformation for about six residues of the arm in those positions where it is not ordered in the compact state. The extended arm and β-annulus of the C-position subunits are conserved. The P-domains are rearranged on the surface of the virus by fairly large rotations about their local diad axes.

The CC P-domain dimer appears to be more disordered than the rest of the structure: the corresponding heavy-atom site refined rather poorly, and the resulting electron density of this domain is considerably weaker than that of the quasi-symmetry-related AB dimer. A model was built with individual relative isotropic temperature factors for the various domains and optimized with respect to the observed dta. The best model had $B = 80$ Å^2 for the A and B position P-domains and $B = 600$ Å^2 for the C position. The latter temperature factor corresponds to a r.m.s. positional fluctuation relative to the S-domains of 5 Å (ref. 19), and because this domain is involved in the inter-particle contact of the crystals it can explain the disorder of the crystals as a whole.

Because of the disorder of the P-domains, it seems unlikely that they are involved in a rigid way with clamping the particle in the expanded state. Moreover, southern bean mosaic virus (SBMV), which has a single domain structurally homologous to the TBSV S-domain and no P-domain[20], also has an expanded particle[21]. If the structural similarity of these viruses extends to the expanded state, the P-domain cannot be specifically involved in the expansion mechanism, and its motions must be a consequence of more fundamental structural changes occurring elsewhere in the virus. The proposed AB S-domain contact (Fig. 5) is a feature that could equally well exist in the expanded state of SBMV as in TBSV.

There is no evidence for ordering of the RNA or the N-terminal portion of the protein, other than the places mentioned. The inter-subunit opening is sufficiently large for the arm to be able to extrude entirely from the virus, even if the N-terminal 65 residues were folded as a third domain of the structure. That some arms do extrude is consistent with their proteolytic sensitivity in expanded TBSV[17].

The expansion mechanism is triggered by deprotonation of the aspartate residues of the calcium binding sites, provided the Ca^{2+} salt bridges have been removed by chelation (Fig. 5). The local build-up of charges must then prise the opening apart. The repulsive force, which would increase monotonically with *p*H in the absence of any induced structural change, is counterbalanced by the attractive forces between domains and between the RNA and the basic amino acids of the interior surface.

Table 2 Final parameters for the best model of expanded TBSV

Translations		Rotations	
x_{SA}	19.4 Å	α_{SA}	4.5°
x_{SBC}	17.8 Å	α_{SBC}	2.1°
x_{PAB}	18.1 Å	α_{PAB}	30°
x_{PC}	14.2 Å	α_{PC}	103°

The parameters are defined in Fig. 1*d* and *e* legends. Direction cosines for AB P-domain dimer translation and rotation. $\vec{c}$, (−0.187, 0.352, 0.917); $\vec{d}$, (−0.264, 0.140, 0.954); θ, 97.1°.

Beyond a critical *p*H, the balance swings in favour of expansion, and the particle switches to its other state by rearrangement of the S-domains. The P-domains then presumably follow suit by adopting minimum-energy configurations on the new surface.

Functions of the structural change

The physiological significance of expansion, if any, is unknown. The expanded state, unlike the compact one, is very sensitive to enzymatic proteolysis, just as it is for BMV[22]. In both cases, this seems to be due to accessibility of normally buried N-terminal sequences. These common features may reflect a common route of entry and disassembly, and Durham[23] has suggested that a difference in calcium concentration between the cytoplasm and the extracellular fluid might be significant in this regard. It is also possible that the expanded state is an intermediate in the virus self-assembly. Whatever its role, the expanded particle demonstrates three additional conformations of the viral subunit. As in the compact structure, the polymorphism is restricted to specific regions of the polypeptide that form specific links between globular domains.

The expansion of TBSV is a highly cooperative change from one state of the viral shell to another: indeed, it has the character of a first-order phase transition[17,24]. There is restructuring of the 2-fold contacts, with conservation of the 5- and 6-fold contacts, giving a two-state character to the transformation. Observed deviations from formal two-state behaviour[17,24] are probably due to changes in the spatially disordered part of the structure, particularly in the N-terminal area. We have strong evidence from the cited proteolytic cleavage experiments[17] that some of these arms extend outside the expanded particle in certain conditions. The manner in which restructured non-covalent contacts are built into the subunit design suggests that the expanded form has a function in the virus life cycle. Indeed, expansion seems to be a general property of small RNA plant viruses. There might also be some formal analogy with the reversiblly interconvertible isoelectric forms of small RNA animal viruses[25].

We thank J. M. Hogle, A. J. Olson, C. S. Steele and D. C. Wiley for advice, discussion and assistance. This research was supported by NIH grant CA-13202.

Received 14 October 1981; accepted 30 March 1982.

1. Ziegler, A., Harrison, S. C. and Leberman, R. *Virology* **59**, 509 (1972).
2. Caspar, D. L. D. & Klug, A. Cold Spring Harb. Symp. quant. Biol. **27**, 1 (1962).
3. Harrison, S. C., Olson, A. J., Schutt, C. E., Winkler, F. K. & Bricogne, G. *Nature* **276**, 368 (1978).
4. Chauvin, C., Witz, J. & Jacrot, B. *J. molec. Biol.* **124**, 641 (1978).
5. Munowitz, M. G., Dobson, C. M., Griffin, R. G. & Harrison, S. C. *J. molec. Biol.* **141**, 327 (1980).
6. Finch, J. T., Klug, A. & Leberman, R. *J. molec. Biol.* **50**, 215 (1970).
7. Incardona, N. L. & Kaesberg, P. *Biophys. J.* **4**, 11 (1964).
8. Bancroft, J. B. *Adv. Virus Res.* **16**, 99 (1970).
9. Caspar, D. L. D. *Adv. Protein Chem.* **18**, 37 (1963).
10. Hogle, J. M., Kirchhausen, T. & Harrison, S. C. *J. molec. Biol.* (submitted).
11. Harrison, S. C. *Biophys. J.* **32**, 139 (1980).
12. McPherson, A. *Meth. Biochem. Analysis* **23**, 249 (1975).
13. Bricogne, G. *Acta crystallogr.* A**30**, 395 (1974).
14. Arndt, U. W. & Wonacott, A. J. *The Rotation Method in Crystallography* (North-Holland, Amsterdam, 1977).
15. Winkler, F. K., Schutt, C. E., Harrison, S. C. & Bricogne, G. *Nature* **265**, 509 (1977).
16. Dickerson, R. E., Kendrew, J. C. & Strandberg, B. E. *Acta crystallogr.* **14**, 1188 (1961).
17. Sorger, P. K., Stockley, P. G., Robinson, I. K. & Harrison, S. C. (in preparation).
18. Stroud, R. M., Kossiakoff, A. A. & Chambers, J. L. *A. Rev. Biophys. Bioengng* **6**, 177 (1977).
19. Debye, P. *Ann. Phys.* **43**, 49 (1914).
20. Abad-Zapatero, C. *et al. Nature* **286**, 33 (1980).
21. Hsu, C. H., White, J. A. & Sehgal, O. P. *Virology* **81**, 471 (1977).
22. Pfeiffer, P. & Hirth, L. *FEBS Lett.* **56**, 144 (1975).
23. Durham, A. C. H., Hendry, D. A. & von Wechmar, M. B. *Virology* **77**, 524 (1977).
24. Kruse, J. & Witz, J. (in preparation).
25. Rueckert, R. R. *Comp. Virol.* **6**, 131 (1976).